Aerosol and Air Quality Research, 19: 422–430, 2019

ISSN: 1680-8584 print / 2071-1409 online
doi: 10.4209/aaqr.2018.06.0215

Deactivation of Ce-Ti Oxide Catalyst by K_3PO_4 for the Selective Catalytic Reduction of NO with NH_3

Ye Jiang[1*], Chengzhen Lai[1], Shaojun Liu[2], Guitao Liang[1], Changzhong Bao[1], Weiyun Shi[1], Shiyuan Ma[1]

[1] *College of Pipeline and Civil Engineering, China University of Petroleum, Qingdao 266580, China*
[2] *State Key Laboratory of Clean Energy Utilization, Zhejiang University, Hangzhou 310027, China*

ABSTRACT

The effect of K_3PO_4 on the selective catalytic reduction of NO with NH_3 over a Ce-Ti oxide catalyst was investigated using XRD, BET, XPS, NH_3-TPD, H_2-TPR and activity measurements. The results showed that K_3PO_4 deactivated the Ce-Ti oxide catalyst seriously. The drop in the amount of Ce^{3+} was accompanied by a decrease in oxygen vacancies and active surface oxygen species, which was disadvantageous to the SCR reaction over the Ce-Ti oxide catalyst. In addition, a reduction in the Brønsted surface acidity and reducibility was also responsible for the deactivation of the Ce-Ti oxide catalyst by K_3PO_4.

Keywords: Selective catalytic reduction; NO; NH_3; K_3PO_4; Ce-Ti oxide; Activity.

INTRODUCTION

Anthropogenic emission of nitrogen oxides (NO_x, x = 1, 2) has attracted extensive concern in recent years because of its serious threat to environment and human health (Li *et al.*, 2017; Yu *et al.*, 2017). Selective catalytic reduction of NO_x with NH_3 (NH_3-SCR) has been considered as one of most effective techniques for NO_x removal in stationary sources. Despite the fact that V_2O_5/TiO_2 mixed with WO_3 or MoO_3 has been industrially applied during the past decades, several drawbacks associated with this type of catalyst have to be noticed, such as toxicity of vanadium species, high oxidization activity of SO_2 to SO_3 (Dunn *et al.*, 1998; Du *et al.*, 2018), formation of greenhouse gas N_2O at high temperatures (Yates *et al.*, 1996) and catalyst deactivation by the exposure to ash compounds present in flue gas (Chen *et al.*, 2011; Jiang *et al.*, 2014; Chen *et al.*, 2018; Wang *et al.*, 2018). Among promising substitutes for commercial V_2O_5/TiO_2-based catalysts, in the last years, considerable attention has been paid to the activities of ceria-based catalysts due to high oxygen storage capacity and outstanding redox property of ceria (Guo *et al.*, 2013; Jiang *et al.*, 2017a; Jiang *et al.*, 2018). From the point of view of industrial applications, it is of great interest to study the influence of flue gas components (e.g., alkali metal, alkaline earth metal, heavy metal, etc.) on the catalytic behaviors of ceria-based catalysts.

As far as the effect of potassium on the SCR of NO with NH_3 over ceria-based SCR catalysts is concerned, previous studies mainly focused on K_2O. Wang *et al.* (2013) reported the strong inhibition by K_2O for the activity of Ce/TiO_2 catalyst. Du *et al.* (2012) attributed the deactivation by K_2O of Ce-Ti oxide to the decrease in its reducibility and surface acidity. Wang *et al.* (2017) revealed that the deposition of K_2O could suppress the adsorption of NH_3 on the surface of Ce/TiO_2 catalyst, thereby resulting in the loss of its activity. Gao *et al.* (2014) compared the effect of K_2O on the SCR activities of ceria supported on zirconia with and without sulfation treatment. Peng *et al.* (2012) proposed that the decrease in the quantity of Brønsted acid sites was responsible for the deactivation by K_2O of CeO_2-WO_3 catalyst. In fact, potassium can be also bound as chloride, sulfate or phosphate, which is largely determined by fuel composition and reaction conditions (Beck *et al.*, 2004; Zhuo *et al.*, 2012; Jang *et al.*, 2016).

Recently, co-combustion of coal with secondary fuels such as municipal sewage sludge, straw, wood or meat and bone meal (MBM) received increasing attention. Considering that these secondary fuels are rich in phosphorus and potassium, their interaction could result in the formation of more potassium phosphate in flue gas during the co-combustion of coal with secondary fuels, compared with coal combustion (Zhuo *et al.*, 2012). Potassium phosphate will be deposited on the surface of SCR catalysts and unavoidably have a further effect on their activities. Because of practical interests, quite a few researchers have investigated the

* Corresponding author.
Tel.: +86-532-86981767; Fax: +86-532-86981882
E-mail address: jiangye@upc.edu.cn

influence of K_3PO_4 on V_2O_5/TiO_2-based catalysts (Beck *et al.*, 2004; Castellino *et al.*, 2009). However, the effect of K_3PO_4 on ceria-based catalysts has been ignored and hardly ever studied until our present work. In addition, different K species would exert a different effect on catalytic behaviors (Zhang *et al.*, 2015; Du *et al.*, 2017). Consequently, it is indispensable to further investigate the effect of K_3PO_4 on the SCR of NO with NH_3 over Ce-Ti oxide catalyst. These catalysts were characterized by means of BET, XRD, XPS, NH_3-TPD, H_2-TPR and catalytic activity measurements in this work.

EXPERIMENTAL

Catalyst Preparation

Ce-Ti oxide was prepared by a single-step sol-gel method and denoted as CT. The CeO_2 loading was set to 20% (the mass ratio of CeO_2/TiO_2). Butyl titanate (0.1 mol), anhydrous ethanol (3.5 mol), deionized water (1.9 mol), nitric acid (0.2 mol) and cerium nitrate (0.01 mol) were mixed and stirred violently at room temperature. After 3 h, the mixture was dried at 80°C for 24 h to form xerogel. At last, the xerogel was calcined at 500°C for 6 h.

The K_3PO_4- and H_3PO_4-doped catalysts were prepared by impregnation via incipient wetness with the aqueous solutions of required concentrations of K_3PO_4 and H_3PO_4 on the Ce-Ti oxide, respectively. The samples were impregnated at room temperature for 4 h. Then the samples were dried at 110°C for 12 h. As for the P_2O_5-doped catalyst, H_3PO_4 was used as the precursor of P_2O_5 and impregnated on the Ce-Ti oxide at room temperature for 4 h. After drying at 110°C for 12 h, the sample was calcined at 500°C for 5 h. A series of K_3PO_4-doped samples were denoted by "KPCT(x)" and "x" was the molar ratio of K to Ce.

Characterization of Catalysts

The physical properties of the samples were measured by N_2 adsorption and desorption at 77 K with ASAP 2020-M (Micromeritics Instrument Corp.). According to the Brunauer-Emmett-Teller (BET) and Barrett-Joyner-Halenda (BJH) methods, BET surface area, total pore volume and average pore diameter could be determined.

X-ray diffraction (XRD) patterns were obtained on an X'Pert PRO MPD system (Panalytical Corp.) with Cu Kα radiation operating at 40 kV and 40 mA. The XRD data were collected in the scattering angles (2θ) ranging between 10 and 90° with a scanning rate of 5° min^{-1}.

The X-ray photoelectron spectroscopy (XPS) spectra were collected on a Thermo ESCALAB 250 spectrometer using monochromated Al Kα X-ray radiation ($h\nu$ = 1486.6 eV) at 150 W. The binding energies of K 2p, Ti 2p, Ce 3d and O 1s were calibrated by measuring the reference peak of C 1s (BE = 284.6 eV) from adventitious carbon in order to eliminate sample charging effect.

The analysis on temperature-programmed desorption (NH_3-TPD) and temperature-programmed reduction (H_2-TPR) were carried out on a FINESORB-3010 chemisorption analyzer (FINETEC Instruments Corp.) with a thermal conductivity detector (TCD).

Catalytic Activity Tests

The SCR activities of the samples were tested in a fixed-bed quartz tubular flow reactor (i.d. = 8 mm) containing 0.34 g catalyst with 60–100 mesh in the temperature range of 150–500°C. The feed gas consisted of 1000 ppm NO, 1000 ppm NH_3, 3% O_2 and balance N_2. The total flow rate was 500 mL min^{-1}, corresponding to a gas hourly space velocity (GHSV) of 90,000 h^{-1}. The concentrations of NO and O_2 were monitored by a flue gas analyzer (350 Pro, Testo). The concentrations of NH_3, N_2O and NO_2 were analyzed by a FT-IR gas analyzer (DX-4000, Gasmet). The activity data were collected and recorded after 30 min when the SCR reaction reached a steady state at each temperature.

RESULTS AND DISCUSSION

SCR Activity Tests

Fig. 1 compares NO conversion as a function of temperatures over Ce-Ti oxides doped with different P species. As for H_3PO_4- and P_2O_5-doped samples, the molar ratio of P/Ce was 0.5:1. Over CT-K_3PO_4, the molar ratio of K/P/Ce was 0.5:0.2:1. It could be seen that the deactivation of CT followed the sequence: CT-P_2O_5 < CT-H_3PO_4 < CT-K_3PO_4. It was clear that different P species would exert a different effect on catalytic behaviors of CT. K_3PO_4 led to most serious deactivation of CT compared with the other two P species. After that, the effect of K_3PO_4 loadings on the catalytic behaviors of CT was investigated and the results are shown in Fig. 2. The catalytic activity of CT deceased with increasing K_3PO_4 loadings in the temperature range of 150–500°C. When the molar ratio of K/Ce reached 0.25, the maximum NO conversion fell to only less than 30% and CT had lost most of its activity. These results indicated that K_3PO_4 acted as a strong inhibitor on the catalytic activity of CT.

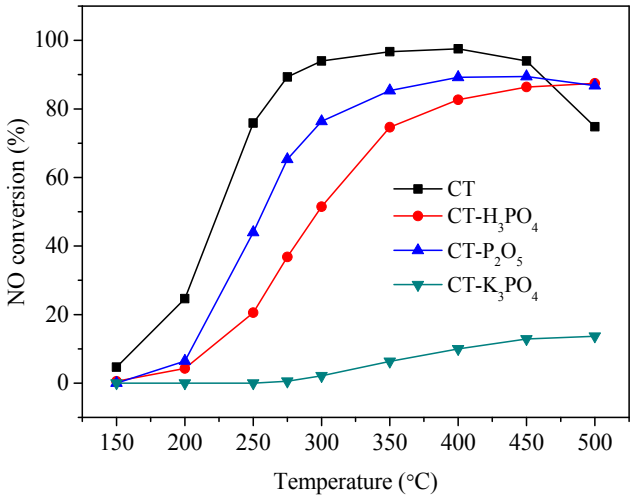

Fig. 1. Variation of NO conversion with temperatures over Ce-Ti oxides doped with different P species. Reaction condition: [NO] = [NH_3] = 1,000 ppm, [O_2] = 3%, N_2 balance, total flow rate = 500 mL min^{-1}, and GHSV = 90,000 h^{-1}.

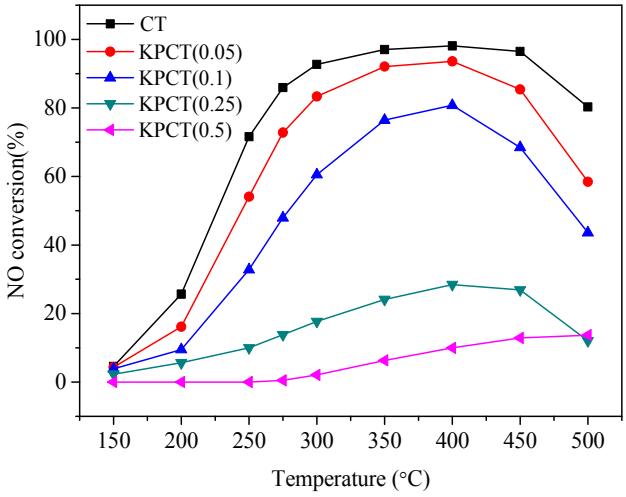

Fig. 2. Variation of NO conversion with temperatures over Ce-Ti oxides with different K_3PO_3 loadings. Reaction condition: [NO] = [NH_3] = 1,000 ppm, [O_2] = 3%, N_2 balance, total flow rate = 500 mL min^{-1}, and GHSV = 90,000 h^{-1}.

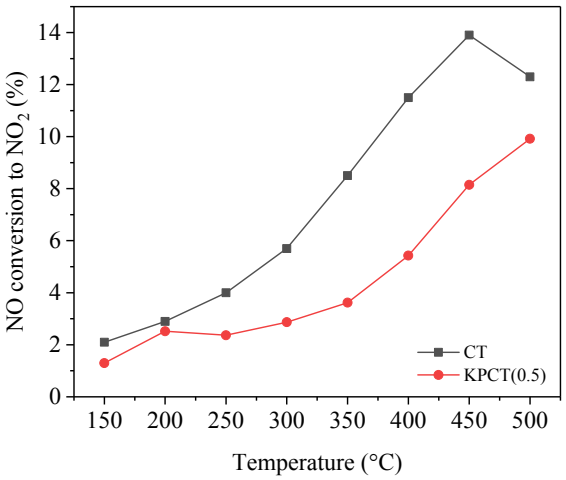

Fig. 3. Oxidation of NO to NO_2 by O_2 over CT and KPCT(0.5). Reaction condition: [NO] = 1,000 ppm, [O_2] = 3%, N_2 balance, total flow rate = 500 mL min^{-1}, and GHSV = 90,000 h^{-1}.

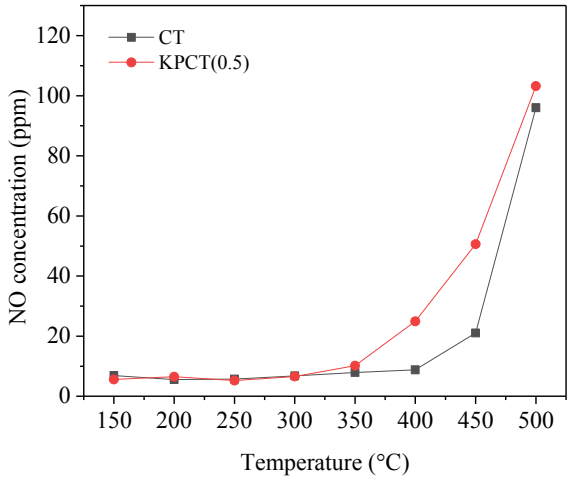

Fig. 4. NO formation over CT and KPCT(0.5). Reaction condition: [NH_3] = 1,000 ppm, [O_2] = 3%, N_2 balance, total flow rate = 500 mL min^{-1}, and GHSV = 90,000 h^{-1}.

The oxidation activities of NO to NO_2 by O_2 were measured over the fresh CT and KPCT(0.5) and the results are presented Fig. 3. As for the fresh CT, the NO oxidation increased with increasing temperatures and reached the maximum of 13.9% at 450°C. Further increasing temperatures led to the drop in the NO oxidation. After adding K_3PO_4, the NO oxidation decreased obviously. It is established that the existence of NO_2 can promote the SCR reaction via the "fast SCR reaction" of $2NH_3 + NO + NO_2 \rightarrow 2N_2 + 3H_2O$ (Fedeyko *et al.*, 2010; Ma *et al.*, 2013). It implied that K_3PO_4 could inhibit the oxidation of NO to NO_2, thereby decreasing the SCR activity of CT.

NH_3 oxidation, as an important side reaction, can cause the decrease in SCR activity at high temperatures (Ma *et al.*, 2013). NH_3 oxidation tests were performed in the feed gas without NO. The concentrations of N_2O and NO_2 were lower than 7 ppm over the two samples in the temperature range of 150–500°C. Therefore, the NH_3 oxidation results only contained the NO concentration curves (see Fig. 4). It could be seen from Fig. 4 that the NH_3 oxidation started at about 350°C and increased sharply with temperatures over the fresh CT. After doping K_3PO_4, NO concentration increased at 350–500°C obviously, while no obvious change was observed below 350°C. This indicated that the presence of K_3PO_4 could result in the formation of more NO at high temperatures, which led to the decrease in the SCR activity of CT.

Characterization of Catalysts

XRD Results

The XRD patterns of Ce-Ti oxides with various K_3PO_4 loadings are illustrated in Fig. 5. For the fresh CT, only anatase TiO_2 could be detected while the characteristic diffraction peaks of Ce species were not found. This indicated that Ce species were well dispersed and existed as an amorphous or highly dispersed phase on the surface of anatase TiO_2. After doping K_3PO_4, the characteristic peaks belonging to Ce, K or P species were not observed. Du *et al.* (2012) found similar phenomena when they studied the effect of K and Na on Ce-Ti oxide prepared by a co-precipitation method. It meant that the dispersion of CeO_2 was barely influenced by K_3PO_4. However, the intensity of the characteristic peaks of anatase TiO_2 was found to decrease over KPCT(0.5). Our previous study found a similar phenomenon over Ca-doped Ce-Ti oxide catalysts (Jiang *et al.*, 2017b). The mean crystallite size of anatase was evaluated using the Scherrer equation. When the molar ratio of K/Ce was lower than 0.5, the grain size of anatase was about 4.8 nm. As for KPCT(0.5), the grain size of anatase decreased to 3.4 nm. The mean crystallite sizes of anatase in different samples agreed well with the XRD results. It indicated that there existed a strong interaction between K_3PO_4 and TiO_2.

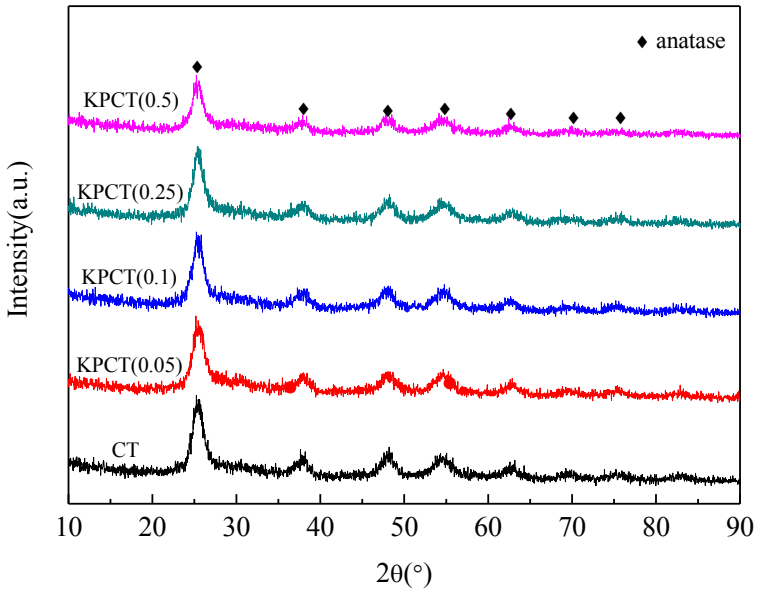

Fig. 5. XRD patterns of Ce-Ti oxides with different K_3PO_3 loadings.

N_2 Adsorption-Desorption Results

Fig. 6 shows the N_2 adsorption-desorption isotherms and corresponding pore size distribution curves of the fresh and K_3PO_4-doped CT catalysts. Both samples had a typical "IV" isotherm, suggestive of mesoporous structures (Leofantia *et al.*, 1998). As shown in Fig. 6(b), the pore distribution of the fresh CT was centered at around 6.2 nm, which could be attributed to the pore structure of the TiO_2 support. After doping K_3PO_4, the pore size was slightly shifted to a higher value while the pore volume decreased a little. It confirmed that the impregnation of K_3PO_4 only caused slight pore blocking.

XPS Results

Table 1 lists the concentration of various atoms on the fresh and K_3PO_4-doped CT catalysts. The presence of K_3PO_4 resulted in the slight decrease in the concentration of active Ce atom from 30.53 at.% to 30.18 at.%. The concentrations of Ti and O were also found to fall, compared with those on the surface of the fresh CT. It seemed probably to be originated from the fact that the catalyst surface might be covered with K_3PO_4 during its impregnation process. K_3PO_4 hindered the XPS detection of Ce, Ti and O atoms, which lay under K_3PO_4. In our previous study on the effect of $PbCl_2$ on V_2O_5/TiO_2, similar phenomena were also observed (Jiang *et al.*, 2014).

Fig. 7 shows XPS spectra of K 2p, Ti 2p, Ce 3d and O 1s. As shown in Fig. 7(a), the binding energy of the $2p_{3/2}$ peak was 293.2 eV in the K 2p XPS spectra of KPCT(0.5). Referring to the handbook of XPS (Wagner *et al.*, 1979), it could be inferred that K existed in the form of K_3PO_4 on the surface of KPCT(0.5).

For the fresh CT, two main peaks ascribed to Ti $2p_{1/2}$ and Ti $2p_{3/2}$ were observed at about 464.5 eV and 458.4 eV, respectively (see Fig. 7(b)). It indicated that Ti was present in the form of Ti^{4+} (Wagner *et al.*, 1979). After doping K_3PO_4, the binding energies of Ti 2p were hardly changed. It implied that the presence of K_3PO_4 had almost no impact on the chemical state of Ti. Ti still existed as Ti^{4+} in KPCT(0.5). However, the intensity of the Ti 2p XPS peaks was found to decrease to a certain extent. This might be ascribed to an interaction between K_3PO_4 and Ti, which was also demonstrated in XRD results.

According to the convention established by Burroughs *et al.* (1976), the XPS spectra of Ce 3d could be deconvoluted into eight overlapped peaks. The peaks labeled as *u′* and *v′* represented the $3d^{10}4f^1$ initial electronic state corresponding to surface Ce^{3+}, while the other ones were assigned to the $3d^{10}4f^0$ initial electronic state of surface Ce^{4+} species (Burroughs *et al.*, 1976). As exhibited in Fig. 7(c), Ce existed in both forms of Ce^{3+} and Ce^{4+} on the surface of the fresh CT. It is widely accepted that the Ce^{3+}/Ce^{4+} pairs contribute to the storage and release of active oxygen species and the oxidation of NO to NO_2 (Geng *et al.*, 2017). Furthermore, a higher Ce^{3+} ratio is indicative of more oxygen vacancies, which help to adsorb reactants (Liu *et al.*, 2013a; Liu *et al.*, 2013b). All of these factors are favorable to the SCR reaction. According to the area ratio of peaks ascribed to Ce^{3+} and Ce^{4+}, the ratio of $Ce^{3+}/(Ce^{3+} + Ce^{4+})$ could be calculated. After doping K_3PO_4, the ratio of $Ce^{3+}/(Ce^{3+} + Ce^{4+})$ decreased from 0.48 to 0.29. It was clear that the amount of Ce^{3+} decreased after doping K_3PO_4. The oxidation state of Ce species on the catalyst surface was changed remarkably. The decrease in the amount of Ce^{3+} resulted from the fact that the interaction between K_3PO_4 and Ce species suppressed the reduction of Ce^{4+} to Ce^{3+} in SCR reaction. Consequently, the reducibility of the CT was lessened. In addition, K_3PO_4 acted as an inhibitor on the electron transfer and resulted in the decrease in the amount of oxygen vacancies, which was disadvantageous to the adsorption and activation of reactive species (Geng *et al.*, 2017). In a word, the decrease in the amount of Ce^{3+} and the degradation of reducibility should be responsible for a strong inhibition of K_3PO_4 in the activity of the Ce-Ti oxide.

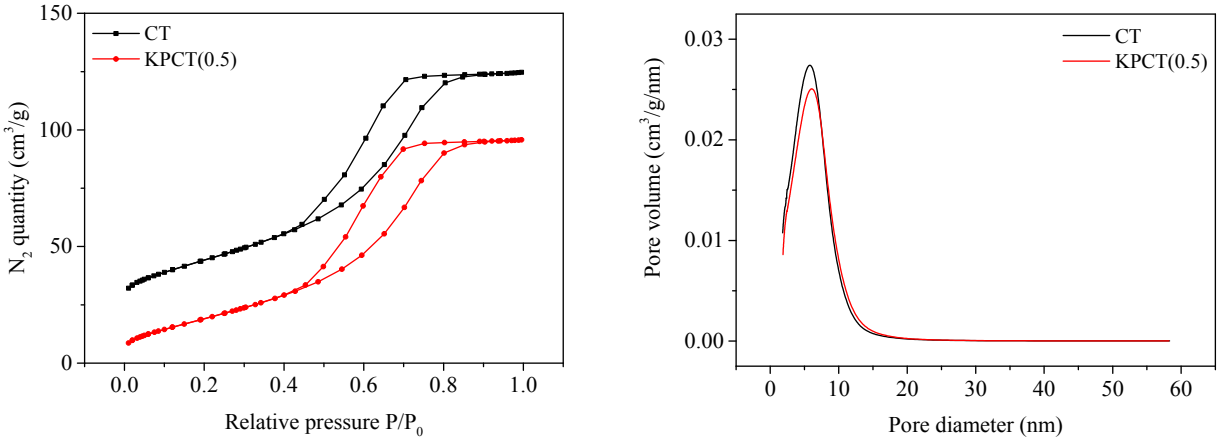

Fig. 6. (a) N_2 adsorption-desorption isotherms and (b) pore size distribution curves of CT and KPCT(0.5).

Table 1. Surface atomic concentration of different elements on fresh and K_3PO_4-doped CT catalysts.

Samples	Surface atomic concentration (at. %)				
	Ce	Ti	O	P	K
CT	30.53	34.43	31.52	-	-
KPCT(0.5)	30.18	32.80	31.43	0.63	3.60

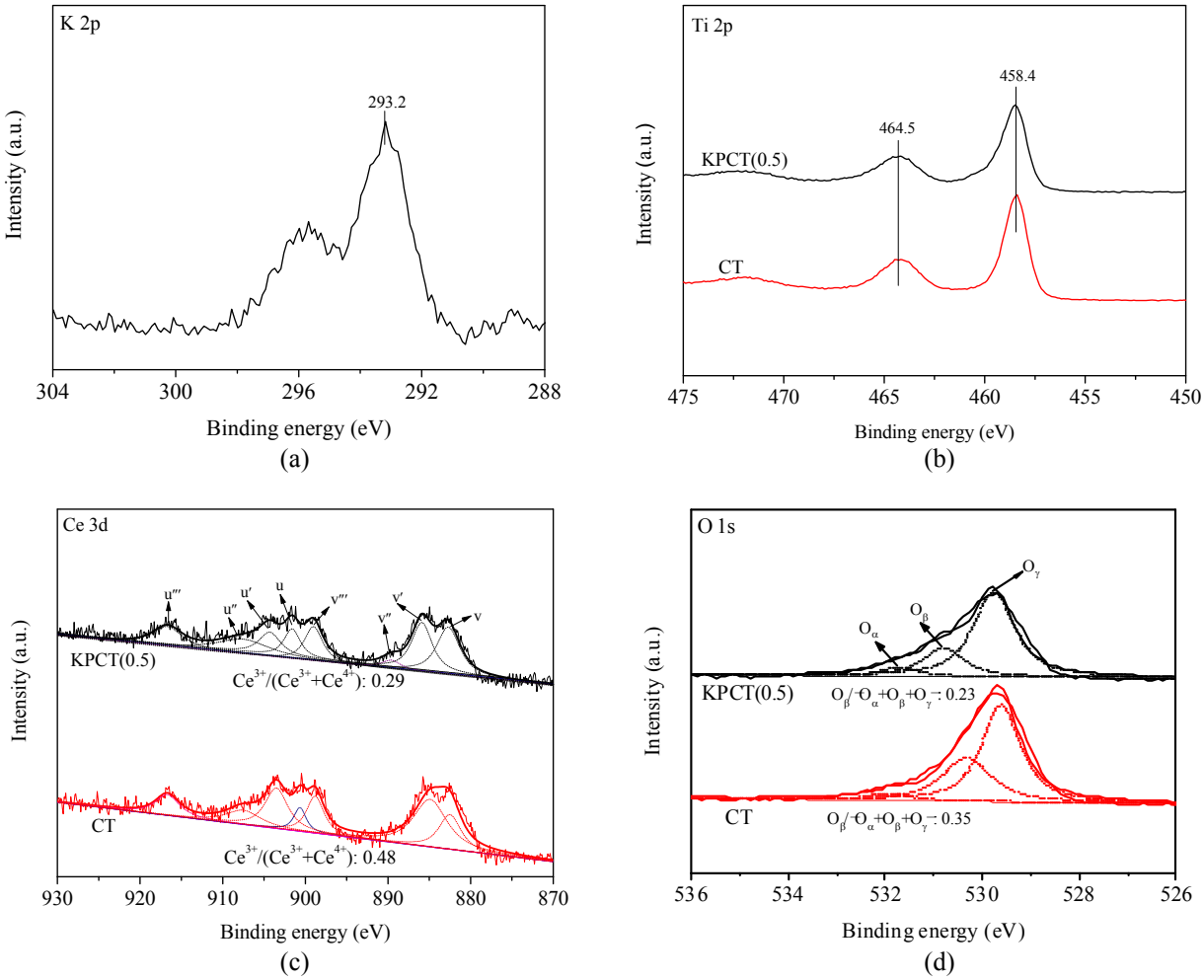

Fig. 7. XPS spectra of (a) K 2p, (b) Ti 2p, (c) Ce 3d, and (d) O 1s of CT and KPCT(0.5).

The O 1s XPS curves of different samples were made up of three overlap peaks, as illustrated in Fig. 7(d). The peaks at 527.7–530.6 eV corresponded to lattice oxygen O^{2-} in the metal oxides (denoted as O_α), the peaks at 530.6–531.1 eV belonged to surface labile oxygen such as O^- or OH from defect-oxide or hydroxyl-like groups (denoted as O_β), and the peaks at 531.1–533.5 eV were assigned as chemisorbed water (denoted as O_γ) (Dupin *et al.*, 2000; Eom *et al.*, 2008; Lee and Bai, 2018). Owing to its higher mobility, O_β is considerably more active than O_α and O_γ (Jiang *et al.*, 2018). High O_β ratio is beneficial for the oxidation of more NO to NO_2 in the SCR process (Wu *et al.*, 2008; Chen *et al.*, 2009). It was reported that the reaction rate of NH_3 with the mixture of NO and NO_2 was faster than that with NO alone, especially at low temperature (Long and Yang, 1999). Therefore, high O_β ratio is indicative of superior SCR activity. After doping K_3PO_4, the ratio of $O_\beta/(O_\alpha + O_\beta + O_\gamma)$ was found to decrease from 0.35 to 0.23, which indicated less surface chemisorbed oxygen on the surface of K_3PO_4-doped CT. This might be due to the fact that potassium ions easily occupied oxygen vacancies since they had similar ionic radius with oxygen ions (Zhang *et al.*, 2014). These results confirmed that the decrease of Ce^{3+} was accompanied by the decrease in oxygen vacancies and active oxygen species, which played a negative role in the SCR activity of CT.

NH_3-TPD Results

NH_3-TPD analysis was performed to study the effect of K_3PO_4 on the surface acidity of CT and the results are shown in Fig. 8. The fresh CT exhibited a broad NH_3 desorption peak in the temperature range of 100–500°C and a small peak at 500–700°C. After deconvolution and peak-fitting, the broad peak could be separated into two peaks centered at about 205°C and 310°C. It is known that the ammonia adsorbed on Brønsted acid sites has less thermal stability than that adsorbed on Lewis acid sites during TPD process (Phil *et al.*, 2008). As a result, the low- and medium-temperature peaks could be assigned to the weak and moderate adsorption of ammonia on Brønsted acid sites (Cai *et al.*, 2014). The small high-temperature peak could be attributed to the NH_3 species strongly adsorbed on Lewis acid sites (Zhao *et al.*, 2016; Duan *et al.*, 2017). It was clear that most of adsorbed NH_3 was coordinated to Brønsted acid sites, which played a predominant role in SCR reaction. After doping K_3PO_4, no significant change was observed on the high-temperature NH_3 desorption peak. This indicated that the Lewis acid sites on the surface of CT were hardly influenced by K_3PO_4. However, the other two peaks shifted to lower temperatures, while their peak areas decreased considerably, especially the medium-temperature peak. Tang *et al.* (2010) also found similar changes on the NH_3-TPD profiles of Na^+-V_2O_5/TiO_2 catalysts. It is accepted that the peak location is closely related to the adsorption strength and the peak area corresponds to the amount of the adsorbed NH_3 (Cai *et al.*, 2014). After doping K_3PO_4, though the NH_3-adsorbed species could be more easily desorbed at low temperatures, the tremendous decrease in the Brønsted acidity resulted in the great weakness of the ability of CT to adsorb NH_3. Ce^{3+} was reported to be related to the formation of Brønsted acid sites (Shu *et al.*, 2012). It would be worthwhile to notice that the decrease in the amount of Ce^{3+} on the surface of K_3PO_4-doped CT had been demonstrated by the above XPS results. Therefore, the significant decrease in the amount of Brønsted acid sites is one of the main reasons for the loss of the activity of CT after doping with K_3PO_4.

H_2-TPR Results

Fig. 9 displays the H_2-TPR profiles of the fresh and K_3PO_4-doped CT catalysts. As for the fresh CT, the onset temperature of reduction was at about 320 °C and there were two overlapped reduction peaks centered at around 515°C and 680°C. The peak at low temperature was probably related to the reduction of the surface oxygen of ceria (Ce^{4+}-O-Ce^{4+}) and the one at high temperature could be attributed to the reduction of Ce^{4+} to Ce^{3+} (Liu *et al.*, 2013a; Liu *et al.*, 2018). In contrast, the onset temperature of reduction shifted to a higher value (about 370°C) and only one reduction peak centered at about 600°C was observed over KPCT(0.5). Higher onset and reduction peak temperatures are generally regarded as indicators of

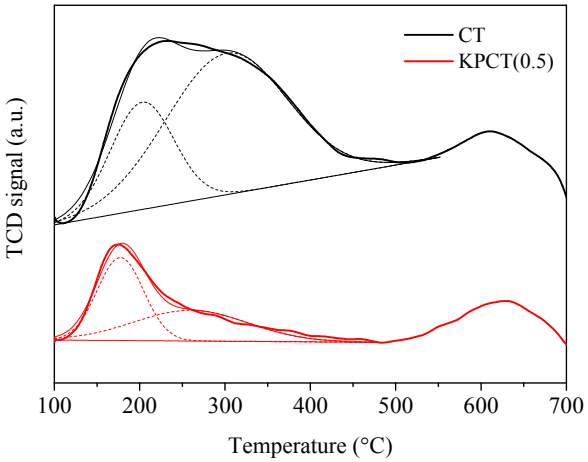

Fig. 8. NH_3-TPD profiles of CT and KPCT(0.5).

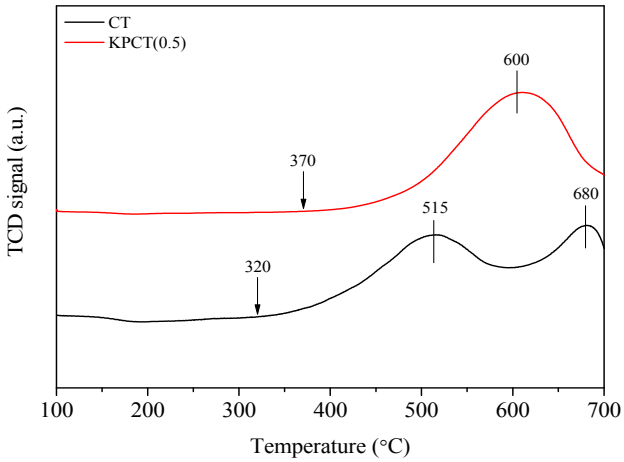

Fig. 9. H_2-TPR profiles of CT and KPCT(0.5).

the decrease in the reducibility (Liu *et al.*, 2008; Gao *et al.*, 2010; Zhao *et al.*, 2016). It was clear that the presence of K_3PO_4 led to the remarkable drop in the reducibility of CT. It should be noted that this result was exactly in line with that of the above XPS analysis. In correlation with the results of BET, XRD and XPS, the loading of K_3PO_4 made the reduction of CT harder probably because of decreased surface area, less surface oxygen, change in chemical state of Ce species and the interaction of K_3PO_4 with Ce species.

CONCLUSIONS

K_3PO_4 deactivated the Ce-Ti oxide catalyst seriously for the selective catalytic reduction of NO with NH_3. The fresh and K_3PO_4-doped Ce-Ti oxides were characterized using XRD, BET, XPS, H_2-TPR and NH_3-TPD. The results indicated that K_3PO_4 had no significant effect on the dispersion and crystalline form of Ce species on anatase TiO_2. After doping the catalyst with K_3PO_4, the BET surface area and total pore volume decreased, and the pore were found to be slightly blocked. The XPS results revealed that the interaction between K_3PO_4 and Ce species hindered the transformation of Ce^{4+} into Ce^{3+}. As a result, the amount of Ce^{3+} decreased, accompanied by a decline in oxygen vacancies and active oxygen species, which played a negative role in the SCR reaction over the Ce-Ti oxide. Both the XPS and the H_2-TPR results demonstrated a decrease in the reducibility of the Ce-Ti oxide after K_3PO_4 doping. In addition, the reduction in surface acidity, mainly due to the decreased number of Brønsted acid sites, may lead to the marked drop in the amount of NH_3 adsorbed on the catalyst surface. Based on these results, the decrease in the amount of Ce^{3+}, oxygen vacancies and surface chemisorbed oxygen and the reduction in surface Brønsted acidity and reducibility were primarily responsible for the deactivation of the Ce-Ti oxide by K_3PO_4.

ACKNOWLEDGEMENTS

This work was supported by the National Natural Science Foundation of China (No. 51506226), Natural Science Foundation of Shandong Province (No. ZR2015EM010), the Fundamental Research Funds for the Central Universities (No. 15CX05005A) and the scholarship from China Scholarship Council, China (CSC) (No. 201706455013).

SUPPLEMENTARY MATERIAL

Supplementary data associated with this article can be found in the online version at http://www.aaqr.org.

REFERENCE

Beck, J., Brandenstein, J., Unterberger, S. and Hein, K.R.G. (2004). Effects of sewage sludge and meat and bone meal co-combustion on SCR catalysts. *Appl. Catal. B* 49: 15–25.

Burroughs, P., Hamnett, A., Orchard, A.F. and Thornton, G. (1976). Satellite structure in the X-ray photoelectron spectra of some binary and mixed oxides of lanthanum and cerium. *J. Chem. Soc. Dalton. Trans.* 17: 1686–1698.

Cai, S., Zhang, S., Zhang, L., Huang, L., Li, H., Gao, R., Shi, L. and Zhang, J. (2014). Comparative study of 3D ordered macroporous $Ce_{0.75}Zr_{0.2}M_{0.05}O_{2-\delta}$ (M=Fe, Cu, Mn, Co) for selective catalytic reduction of NO with NH_3. *Catal. Sci. Technol.* 4: 93–101.

Castellino, F., Jensen, A.D., Johnsson, J.E. and Fehrmann, R. (2009). Influence of reaction products of K-getter fuel additives on commercial vanadia-based SCR catalysts: Part I. Potassium phosphate. *Appl. Catal. B* 86: 196–205.

Chen, L., Li, J. and Ge, M. (2009). Promotional effect of Ce-doped V_2O_5-WO_3/TiO_2 with low vanadium loadings for selective catalytic reduction of NO_x by NH_3. *J. Phys. Chem. C* 113: 21177–21184.

Chen, L., Li, J. and Ge, M. (2011). The poisoning effect of alkali metals doping over nano V_2O_5-WO_3/TiO_2 catalysts on selective catalytic reduction of NO_x by NH_3. *Chem. Eng. J.* 170: 531–537.

Chen, Y., Wang, M., Du, X., Ran, J., Zhang, L. and Tang, D. (2018). High resistance to Na poisoning of V_2O_5-$Ce(SO_4)_2/TiO_2$ catalyst for the NO SCR reaction. *Aerosol Air Qual. Res.* 18: 2948–2955.

Du, X., Gao, X., Qu, R., Ji, P., Luo, Z. and Cen, K. (2012). The influence of alkali metals on the Ce-Ti mixed oxide catalyst for the selective catalytic reduction of NO_x. *ChemCatChem* 4: 2075–2081.

Du, X., Yang, G., Chen, Y., Ran, J. and Zhang, L. (2017). The different poisoning behaviors of various alkali metal containing compounds on SCR catalyst. *Appl. Surf. Sci.* 392: 162–168.

Du, X., Xue, J., Wang, X., Chen, Y., Ran, J. and Zhang, L. (2018). Oxidation of sulfur dioxide over V_2O_5/TiO_2 catalyst with low vanadium loading: A theoretical study. *J. Phys. Chem. C* 122: 4517–4523.

Duan, Z., Chi, K., Liu, J., Shi, J., Zhao, Z., Wei, Y. and Song, W. (2017). The catalytic performances and reaction mechanism of nanoparticle Cd/Ce-Ti oxide catalysts for NH_3-SCR reaction. *RSC Adv.* 7: 50127–50134.

Dunn, J.P., Koppula, P.R., Stenger, H.G. and Wachs, I.E. (1998). Oxidation of sulfur dioxide to sulfur trioxide over supported vanadia catalysts. *Appl. Catal. B* 19: 103–117.

Dupin, J.C., Gonbeau, D., Vinatier, P. and Levasseur, A. (2000). Systematic XPS studies of metal oxides, hydroxides and peroxides. *Phys. Chem. Chem. Phys.* 2: 1319–1324.

Eom, Y., Jeon, S.H., Ngo, T.A., Kim, J. and Lee, T.G. (2008). Heterogeneous mercury reaction on a selective catalytic reduction (SCR) catalyst. *Catal. Lett.* 121: 219–225.

Fedeyko, J.M., Chen, B. and Chen, H. (2010). Mechanistic study of the low temperature activity of transition metal exchanged zeolite SCR catalysts. *Catal. Today* 151: 231–236.

Gao, S., Wang, P., Chen, X., Wang, H., Wu, Z. and Li, Y. (2014). Enhanced alkali resistance of CeO_2/SO_4^{2-}-ZrO_2 catalyst in selective catalytic reduction of NO_x by ammonia. *Catal. Commun.* 43: 223–226.

Gao, X., Jiang, Y., Fu, Y., Zhong, Y., Luo, Z. and Cen, K. (2010). Preparation and characterization of CeO_2/TiO_2 catalysts for selective catalytic reduction of NO with NH_3. *Catal. Commun.* 11: 465–469.

Geng, Y., Chen, X., Yang, S., Liu, F. and Shan, W. (2017). Promotional effects of Ti on a CeO_2-MoO_3 catalyst for the selective catalytic reduction of NO_x with NH_3. *Appl. Mater. Interfaces* 9: 16951–16958.

Guo, R., Zhou, Y., Pan, W., Hong, J., Zheng, W., Jin, Q., Ding, C. and Guo, S. (2013). Effect of preparation methods on the performance of CeO_2/Al_2O_3 catalysts for selective catalytic reduction of NO with NH_3. *J. Ind. Eng. Chem.* 19: 2022–2025.

Jang, H., Kim, J., Back, S., Sung, J., Yoo, H., Choi, H.S. and Seo, Y. (2016). Combustion characteristics of waste sludge at air and oxy-fuel combustion conditions in a circulating fluidized bed reactor. *Fuel* 170: 92–99.

Jiang, Y., Gao, X., Zhang, Y., Wu, W., Song, H., Luo, Z. and Cen, K. (2014). Effects of $PbCl_2$ on selective catalytic reduction of NO with NH_3 over vanadia-based catalysts. *J. Hazard. Mater.* 274: 270–278.

Jiang, Y., Wang, X., Xing, Z., Bao, C. and Liang, G. (2017a). Preparation and characterization of CeO_2-MoO_3/TiO_2 catalysts for selective catalytic reduction of NO with NH_3. *Aerosol Air Qual. Res.* 17: 2726–2734.

Jiang, Y., Wang, X., Bao, C., Huang, S., Zhang, X. and Wang, X. (2017b). Poisoning effect of CaO on CeO_2/TiO_2 catalysts for selective catalytic reduction of NO with NH_3. *Korean J. Chem. Eng.* 34: 1874–1881.

Jiang, Y., Bao, C., Liu, S., Liang, G., Lu, M., Lai, C., Shi, W. and Ma, S. (2018). Enhanced activity of Nb-modified CeO_2/TiO_2 catalyst for the selective catalytic reduction of NO with NH_3. *Aerosol Air Qual. Res.* 18: 2121–2130.

Lee, T. and Bai, H. (2018). Metal Sulfate Poisoning effects over $MnFe/TiO_2$ for selective catalytic reduction of NO by NH_3 at low temperature. *Ind. Eng. Chem. Res.* 57: 4848–4858.

Leofantia, G., Padovanb, M., Tozzolac, G. and Venturellic, B. (1998). Surface area and pore texture of catalysts. *Catal. Today* 41: 207–219.

Li, Q., Liu, H., Chen, T., Chen, D., Zhang, C., Xu, B., Zhu, C. and Jiang, Y. (2017). Characterization and SCR performance of nano-structured iron-manganese oxides: Effect of annealing temperature. *Aerosol Air Qual. Res.* 17: 2328–2337.

Liu, C., Chen, L., Chang, H., Ma, L., Peng, Y., Arandiyan, H. and Li, J. (2013a). Characterization of CeO_2-WO_3 catalysts prepared by different methods for selective catalytic reduction of NO_x with NH_3. *Catal. Commun.* 40: 145–148.

Liu, J., Zhao, Z., Wang, J., Xu, C., Duan, A., Jiang, G. and Yang, Q. (2008). The highly active catalysts of nanometric CeO_2-supported cobalt oxides for soot combustion, *Appl. Catal. B* 84: 185–195.

Liu, Z., Yi, Y., Li, J., Woo, S.I., Wang, B., Cao, X. and Li, Z. (2013b). A superior catalyst with dual redox cycles for the selective reduction of NO_x by ammonia. *Chem. Commun.* 49: 7726–7728.

Liu, Z., Feng, X., Zhou, Z., Feng, Y. and Li, J. (2018). Ce-Sn binary oxide catalyst for the selective catalytic reduction of NO_x by NH_3. *Appl. Surf. Sci.* 428: 526–533.

Long, R. and Yang, R.T. (1999). Catalytic Performance of Fe-ZSM-5 catalysts for selective catalytic reduction of nitric oxide by ammonia. *J. Catal.* 188: 332–339.

Ma, Z., Yang, H., Liu, F. and Zhang, X. (2013). Interaction between SO_2 and Fe-Cu-O_x/CNTs-TiO_2 catalyst and its influence on NO reduction with NH_3. *Appl. Catal. A* 467: 450–455.

Peng, Y., Li, J., Chen, L., Chen, J., Han, J., Zhang, H. and Han, W. (2012). Alkali metal poisoning of a CeO_2-WO_3 catalyst used in the selective catalytic reduction of NO_x with NH_3: An experimental and theoretical study. *Environ. Sci. Technol.* 46: 2864–2869.

Phil, H.H., Reddy, M.P., Kumar, P.A., Ju, L.K. and Hyo, J.S. (2008). SO_2 resistant antimony promoted V_2O_5/TiO_2 catalyst for NH_3-SCR of NO_x at low temperatures. *Appl. Catal. B* 78: 301–308.

Shu, Y., Sun, H., Quan, X. and Chen, S. (2012). Enhancement of catalytic activity over the iron-modified Ce/TiO_2 catalyst for selective catalytic reduction of NO_x with ammonia. *J. Phys. Chem. C* 116: 25319–25327.

Tang, F., Xu, B., Shi, H., Qiu, J. and Fan, Y. (2010). The poisoning effect of Na^+ and Ca^{2+} ions doped on the V_2O_5/TiO_2 catalysts for selective catalytic reduction of NO by NH_3. *Appl. Catal. B* 94: 71–76.

Wagner, C.D., Riggs, W.M., Davis, L.E., Moulder, J.F. and Mullenberg, G.E. (1979). *Handbook of X-ray photoelectron spectroscopy*, Perkin-Elmer Corporation, Minnesota, USA.

Wang, H., Chen, X., Gao, S., Wu, Z., Liu, Y. and Weng, X. (2013). Deactivation mechanism of Ce/TiO_2 selective catalytic reduction catalysts by the loading of sodium and calcium salts. *Catal. Sci. Technol.* 3: 715–722.

Wang, S., Guo, R., Pan, W., Chen, Q., Sun, P., Li, M. and Liu, S. (2017). The deactivation of Ce/TiO_2 catalyst for NH_3-SCR reaction by alkali metals: TPD and DRIFT studies. *Catal. Commun.* 89: 143–147.

Wang, X., Du, X., Zhang, L., Chen, Y., Yang, G. and Ran, J. (2018). Promotion of NH_4HSO_4 decomposition in NO/NO_2 contained atmosphere at low temperature over V_2O_5-WO_3/TiO_2 catalyst for NO reduction. *Appl. Catal. A* 559: 112–121.

Wu, Z., Jin, R., Liu, Y. and Wang, H. (2008). Ceria modified MnO_x/TiO_2 as a superior catalyst for NO reduction with NH_3 at low-temperature. *Catal. Commun.* 9: 2217–2210.

Yates, M., Martín, J.A., Martín-Luengo, M.Á., Suárez, S. and Blanco, J. (1996). N_2O formation in the ammonia oxidation and in the SCR process with V_2O_5-WO_3 catalysts. *Catal. Today* 107–108: 120–125.

Yu, X., Cao, F., Zhu, X., Zhu, X., Gao, X., Luo, Z. and Cen, K. (2017). Characterization and SCR performance of nano-structured iron-manganese oxides: Effect of annealing temperature. *Aerosol Air Qual. Res.* 17: 302–313.

Zhang, L., Cui, S., Guo, H., Ma, X. and Luo, X. (2014). The influence of K^+ cation on the MnO_x-CeO_2/TiO_2 catalysts for selective catalytic reduction of NO_x with

NH_3 at low temperature. *J. Mol. Catal. A* 390: 14–21.

Zhang, L., Cui, S., Guo, H., Ma, X. and Luo, X. (2015). The poisoning effect of potassium ions doped on MnO_x/TiO_2 catalysts for low-temperature selective catalytic reduction. *Appl. Surf. Sci.* 355: 1116–1122.

Zhao, K., Han, W., Lu, G., Lu, J., Tang, Z. and Zhen, X. (2016). Promotion of redox and stability features of doped Ce-W-Ti for NH_3-SCR reaction over a wide temperature range. *Appl. Surf. Sci.* 379: 316–322.

Zhuo, J., Li, S., Duan, L. and Yao, Q. (2012). Effect of phosphorus transformation on the reduction of particulate matter formation during co-combustion of coal and sewage sludge. *Energy Fuels* 26: 3162–3166.

Received for review, July 2, 2018
Revised, November 20, 2018
Accepted, December 10, 2018